Precision Engineering 40 (2015) 172–181

Contents lists available at ScienceDirect

Precision Engineering

journal homepage: www.elsevier.com/locate/precision

Experimental study of crystal anisotropy based on ultra-precision cylindrical turning of single-crystal calcium fluoride

Shunya Azami [a,*], Hiroshi Kudo [b], Yuta Mizumoto [a], Takasumi Tanabe [b], Jiwang Yan [c], Yasuhiro Kakinuma [a]

[a] Department of System Design Engineering, Faculty of Science and Technology, Keio University, 3-14-1 Hiyoshi, Kohoku-ku, Yokohama 223-8522, Japan
[b] Department of Electronics and Electrical Engineering, Faculty of Science and Technology, Keio University, 3-14-1 Hiyoshi, Kohoku-ku, Yokohama 223-8522, Japan
[c] Department of Mechanical Engineering, Faculty of Science and Technology, Keio University, 3-14-1 Hiyoshi, Kohoku-ku, Yokohama 223-8522, Japan

ARTICLE INFO

Article history:
Received 19 August 2014
Received in revised form 25 October 2014
Accepted 10 November 2014
Available online 29 November 2014

Keywords:
Ultra-precision cylindrical turning
Single-crystal calcium fluoride
Crystal anisotropy
Surface quality
Micro-Vickers
Orthogonal cutting

ABSTRACT

To realize ultimately efficient signal processing, it is necessary to replace electrical signal processing circuits with optical ones. The optical micro-resonator, which localizes light at a certain spot, is an essential component in optical signal processing. Single-crystal calcium fluoride (CaF_2) is the most suitable material for a highly efficient optical micro-resonator. The CaF_2 resonator can only be manufactured by ultra-precision machining processes, because its crystal anisotropy does not allow the application of chemical etching. However, the optical micro-resonator's performance depends definitely on the surface integrity.

This study investigated the relationship between surface quality after ultra-precision machining and crystal anisotropy. Firstly, crack initiation was investigated on the (1 0 0), (1 1 0), and (1 1 1) planes using the micro-Vickers hardness test. Secondly, brittle-ductile transition was investigated by orthogonal cutting tests. Finally, cutting performance of cylindrical turning was evaluated, which could be a suitable method for manufacturing the CaF_2 resonator. The most difficult point in cylindrical turning of CaF_2 is that the crystalline plane and cutting direction vary continuously. In order to manufacture the CaF_2 optical micro-resonator more efficiently, analysis was conducted on crack initiation and surface quality of all crystallographic orientations from the perspective of slip system and cleavage.

1. Introduction

The development of the optical transmission technique has increased the transmission speed of communication devices dramatically. Although a signal is transmitted as an optical signal, it currently needs to be converted into an electrical signal for signal processing purposes. Transmission speed decreases in electrical signal processing and energy loss occurs in an integrated circuit through heat. Extremely high processing speed and a reduction in energy loss could be achieved if a conventional signal processing circuit was replaced by an optical one. Optical micro-resonators localize light at certain spots and are essential for optical signal processing. While various semiconductor materials such as Silicon or SiO_2 are utilized for optical micro-resonators [1–3], CaF_2 [4] could be the most suitable material from an absorption coefficient viewpoint. Etching and irradiating with a CO_2 laser have been generally employed for the manufacturing process. However, the application of these processes to CaF_2 is hindered by two problems: the difficultly in controlling anisotropic etching for fabrication of a bulge-shaped resonator [5] and breakage of a single-crystal structure by laser heat. Additionally, the actual performance of the CaF_2 optical micro-resonator fabricated by these processes becomes lower than ideal.

The prospective and feasible CaF_2 resonator fabrication technique is ultra-precision turning and polishing, as shown by Maleki [6,7]. Although the polishing process is required to make the surface of a resonant part smoother, prolonged polishing reduces form accuracy. To shorten polishing time, it is necessary to make a smoother surface at the ultra-precision cutting process stage [8–11]. In addition, the single-crystal CaF_2's characteristics indicate hard brittleness and crystal anisotropy [12–14]. Yan [15] showed that crack initiation depended on cutting direction and that the

* Corresponding author. Tel.: +81 45 566 1657; fax: +81 45 566 1657.
E-mail address: azami@ams.sd.keio.ac.jp (S. Azami).

http://dx.doi.org/10.1016/j.precisioneng.2014.11.007
0141-6359/

critical depth of cut changed remarkably on the basis of the crystal orientation. Previous CaF_2 machining studies have focused on face turning, and showed that the crystalline plane was set to constant. For cylindrical turning on the other hand, which is the fabrication technique for the bulge-shaped resonator, the crystalline plane and cutting direction vary continuously.

The objective of this study was to analyze crack initiation and surface quality in terms of crystal anisotropy. Firstly, a micro-Vickers hardness test was performed to investigate the hardness and plastic deformation of CaF_2 on the (1 0 0), (1 1 0) and (1 1 1) plane. Secondly, orthogonal CaF_2 cutting tests were performed to examine brittle-ductile transition and the critical depth of cut. Finally, cylindrical turning was performed on CaF_2 workpieces with three crystal structures: end face orientation (1 1 1), (1 1 0), and (1 0 0). As crystalline plane and cutting direction vary continuously, crack initiation and surface quality could be analyzed from the perspective of slip system and cleavage for all crystallographic orientations.

2. Micro-Vickers test

2.1. Experimental setup

A micro-Vickers hardness test [16] was performed with a hardness testing machine (MVK-H12, Akashi), which enabled to control the load force (0.05–10 N). A CaF_2 workpiece (38.0 mm × 13.0 mm × 1.0 mm) was pre-polished to remove existing micro-cracks. The pyramidal shape of the indenter had an angle of 136° between opposite faces. It is important for crystalline material machining to produce plastic deformation and prevent crack initiation caused by cleavage. CaF2 generally has a fluorite-type crystal structure, in which the cleavage plane is {1 1 1} and the slip system is {1 0 0} < 1 1 0>. In this test, the plastic deformation and crack initiation mechanisms were investigated from the slip system and cleavage perspective.

Table 1
Angles between each plane of a calcium fluoride structure.

Crystal plane	Angle between crystal plane orientation and slip plane	Angle between crystal plane orientation and cleavage plane
1 0 0	0.0, 90.0°	54.7°
1 1 0	45.0, 90.0°	35.5, 90.0°
1 1 1	54.7°	70.5, 109.5°

2.2. Plastic deformation and crack initiation

Fig. 1 shows the initiation of a crack on each plane viewed through an optical microscope (VH-Z100UR and VH-Z450, KEYENCE). Single-crystal CaF_2 exhibits a cubic structure (calcium fluoride structure). The angles of the slip and cleavage plane are listed in Table 1. In a general micro-Vickers hardness test, a crack appeared along the indenter corner and no cracks appeared along the indenter ridgeline. A crack emanated at load forces of 0.5, 1.0, and 5.0 N on the (1 1 0), (1 1 1) and (1 0 0) planes, respectively. Fig. 2 illustrates the mechanism of plastic deformation corresponding to the slip system and cleavage. On the (1 1 0) plane, cleavage planes existed at an angle of 0°, which corresponded to the indentation

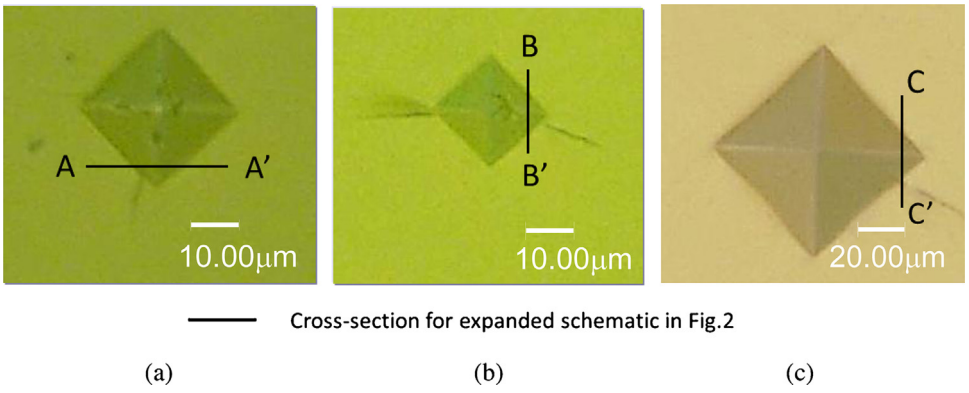

Fig. 1. Optical microscope images of the indentation, for (a) the (1 1 1) plane with a 1.0 N load force, (b) the (1 1 0) plane with a 0.5 N load force, and (c) the (1 0 0) plane with a 5.0 N load force.

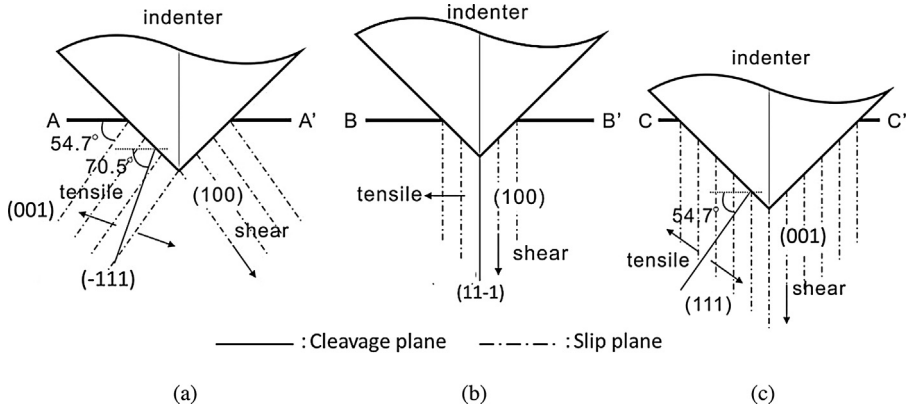

Fig. 2. Expanded schematic overview of the crack initiation mechanism, with (a) the (1 1 1), (b) the (1 1 0), and (c) the (1 0 0) plane.

Table 2
Cutting conditions.

Crystal plane:	(1 1 1), (1 1 0), (1 0 0)	Lubricant:	Kerosine (liquid)
Feed rate mm/min:	100–200	Depth of cut μm:	0–2.0
Cutting direction°:	0–150	D/L:	1/500

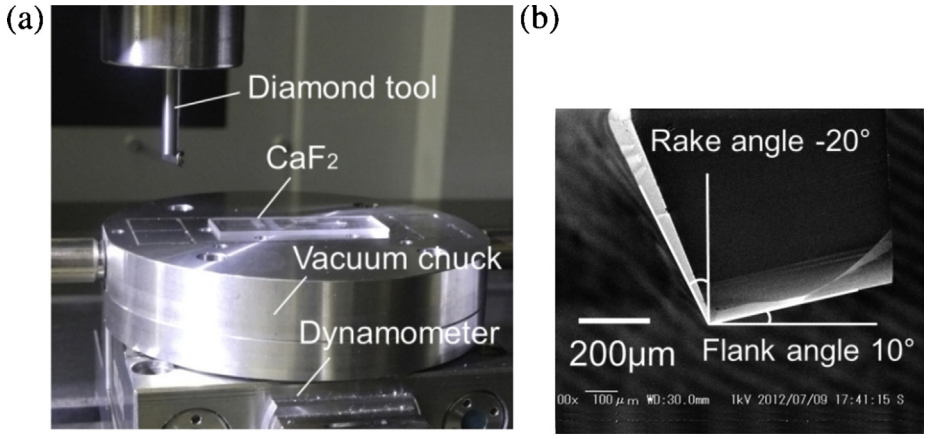

Fig. 3. (a) Experimental set-up, and (b) the single-crystal diamond tool.

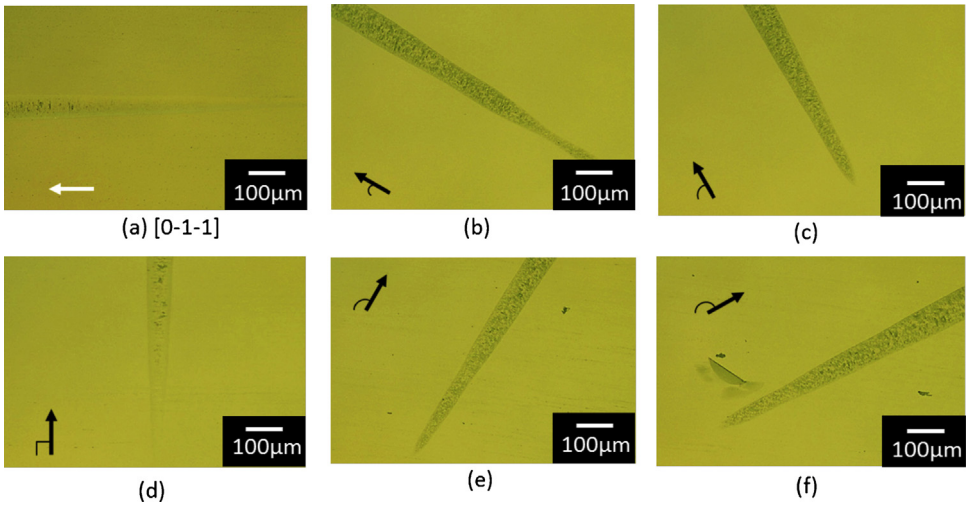

Fig. 4. Machined surfaces of the (100) plane after orthogonal cutting, for a cutting direction of (a) 0°, (b) 30°, (c) 60°, (d) 90°, (e) 120°, and (f) 150°.

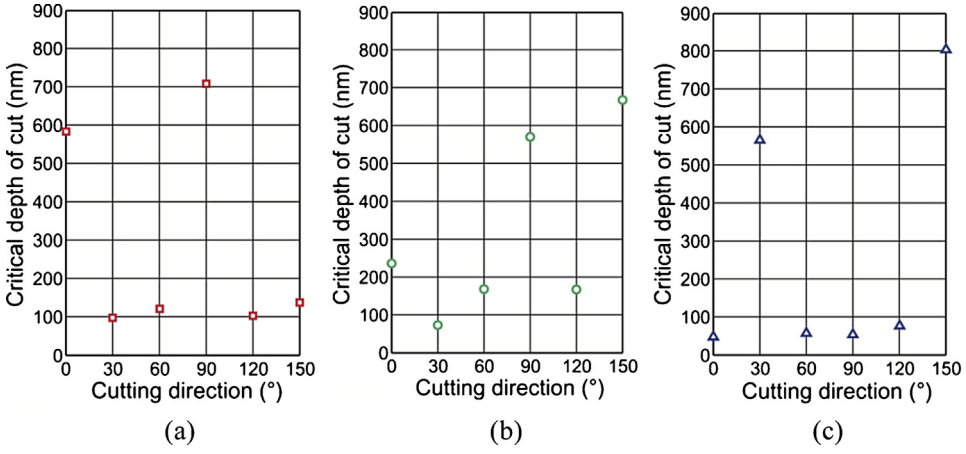

Fig. 5. Critical cut depth versus cutting direction, for (a) the (1 0 0), (b) the (1 1 0), and (c) the (1 1 1) plane.

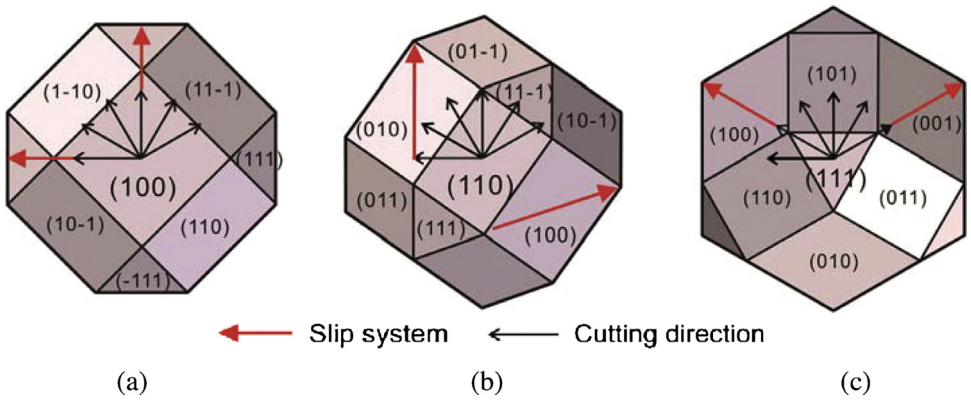

Fig. 6. Crystallographic image of the machined surface, for (a) the (1 0 0), (b) the (1 1 0), and (c) the (1 1 1) plane.

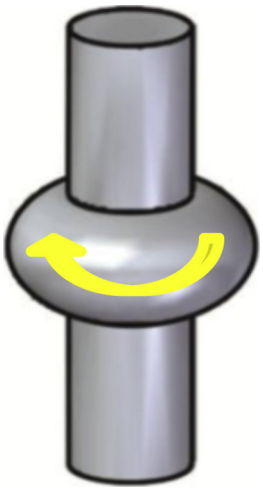

Fig. 7. Geometrical type WGM resonator.

direction. In cleavage planes, tensile stress aided, resulting in crack emanation at loads of just 0.5 N. Additionally, on the (1 1 1) plane, the cleavage plane was closer to the indentation direction than on the slip plane. Cleavage therefore tended to take place and crack initiation occurred at 1.0 N loads. For the (1 0 0) plane, the slip plane (0 0 1) corresponded to the indentation direction. Plastic deformation was therefore generated more easily and a crack did not tend to occur on the (1 0 0) plane like on the other two planes. It was clarified that the slip system and cleavage were strongly related to crack initiation.

3. Orthogonal cutting test

3.1. Experimental setup

An orthogonal cutting test [17] was carried out to investigate the cutting mode transition from ductile to brittle in relation to the depth of cut. A three-axis ultra-precision vertical machine tool

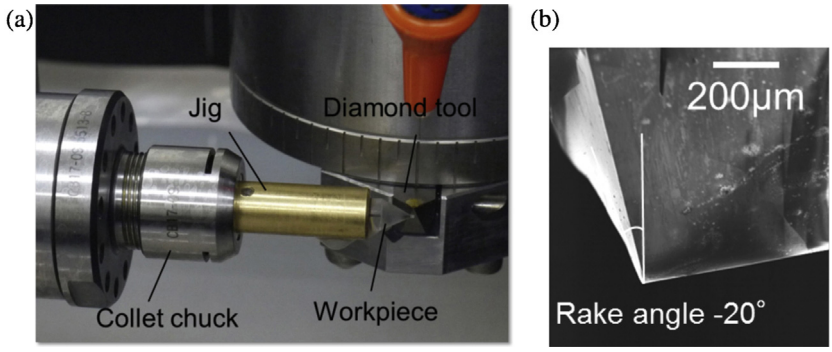

Fig. 8. (a) Experimental setup and (b) single-crystal diamond tool.

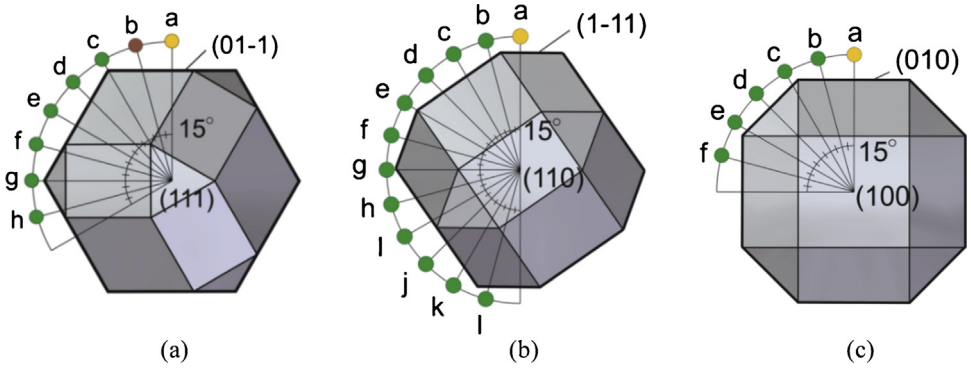

Fig. 9. Crystallographic image of the observation point viewed from the end face, for end face (a) (1 1 1), (b) (1 1 0), and (c) (1 0 0).

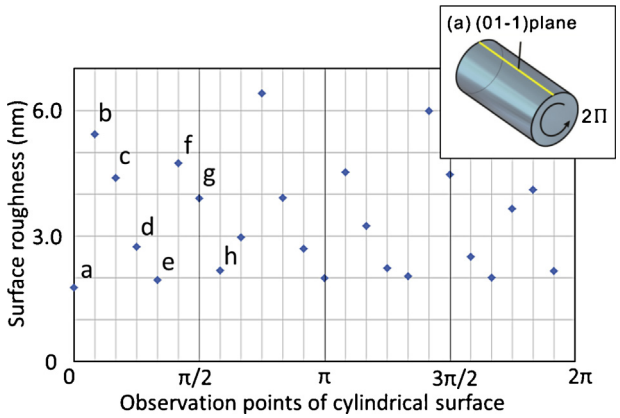

Fig. 10. Cylindrical surface roughness after turning with end face (1 1 1).

(UVM-450C, TOSHIBA MACHINE) was used. The tilt ratio D/L (increment in the depth of cut per unit cutting length) was adjusted to 1/500, which meant that the scratch length was 5 mm and the maximum depth of cut was 10 μm. This tilt ratio was actually set according to the relationship between the *y*- and *z*-axis feed rate by a numerical control (NC) program. The cutting conditions are listed in Table 2. A scanning electron microscope (SEM-VE7800, KEYENCE) image of the single-crystal diamond tool (with a 0.5 mm nose radius, −20° rake [18], 10° flank, and (1 0 0) rake face) is shown in Fig. 3(b). The workpiece was fixed on a holder stage by the vacuum chuck (Fig. 3(a)). The workpiece holder consisted of a base plate, dynamometer, adapter plate, and a vacuum chuck. After the orthogonal cutting test, the machined plane was observed under the optical microscope and the depth of cut was measured under a scanning white light interferometer (New View TM6200, Zygo).

3.2. Critical depth of cut corresponding to crystal orientation

To investigate critical depth of cut according to crystal orientation, orthogonal cutting tests were performed in each 30° cutting direction on each plane. Fig. 4 shows the microscopic images of the machined surface on the (1 0 0) plane in each cutting direction, with the criterion set to the [0−1−1]. Cracks appeared to initiate according to cutting direction. Fig. 5 shows the relationship between critical depth of cut and cutting direction on each plane, which are the (1 0 0), (1 1 0), and (1 1 1) plane. Fig. 6 illustrates the crystallographic images of each machined plane. On the (1 0 0) machined plane, the critical depth of cut became deeper in the 0° and 90° cutting directions (Fig. 5(a)). These cutting directions coincided with the slip system, which could lead to plastic deformation. On the (1 1 0) and (1 1 1) planes, the slip system (shown with the

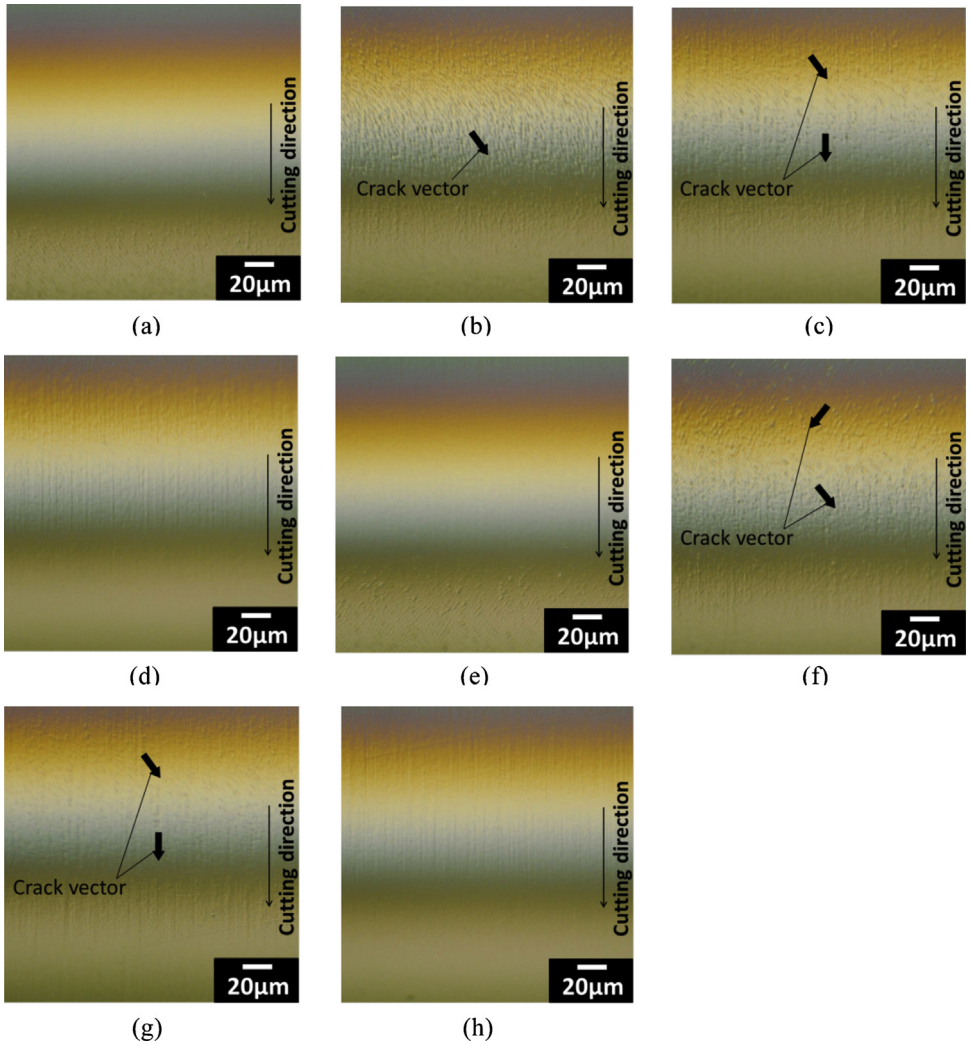

Fig. 11. Machined cylindrical surfaces with end face (1 1 1), for (a) (0 1 −1) [−1 1 1], (b) (−3 11 8) [−1 07 13], (c) (1 2 1) [8 3 15], (d) (8 11 −3) [−3 0 8], (e) (−1 1 0) [−1 −1 1], (f) (−11 8 3) [−7 −13 10], (g) (−211) [−3 −15 8] and (h) (−11 3 8) [0 −8 3].

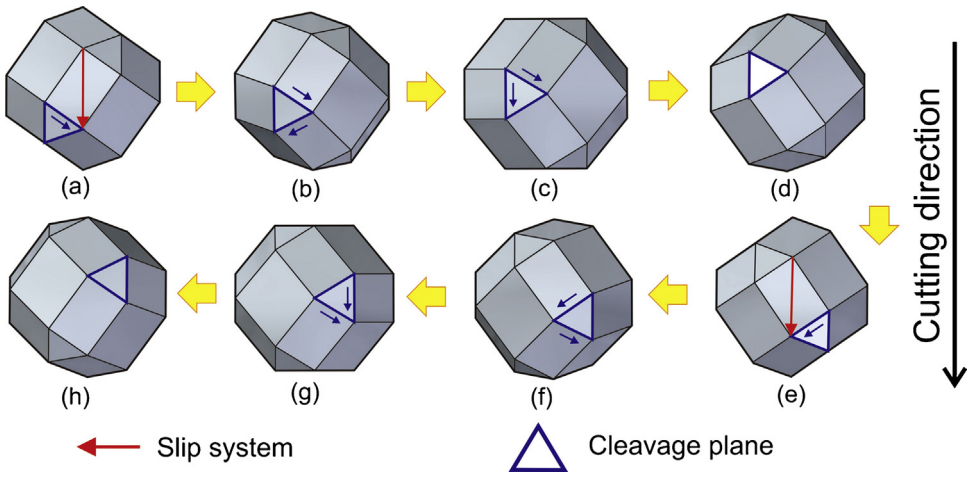

Fig. 12. Crystallographic images of machined cylindrical surfaces with end face (1 1 1), for (a) (0 1 −1) [−1 1 1], (b) (−3 11 8) [−1 07 13], (c) (1 2 1) [8 3 15], (d) (8 11 −3) [−3 0 8], (e) (−1 1 0) [−1 −1 1], (f) (−11 8 3) [−7 −13 10], (g) (−2 1 1) [−3 −15 8] and (h) (−11 3 8) [0 −8 3].

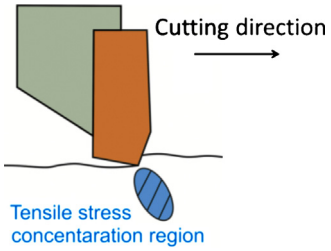

Fig. 13. Schematic view of the tensile stress state during cylindrical rough turning.

red arrow) might have influenced the deeper critical depth of cut. As a result, the critical depth of cut needs to be set below 50 nm, which lead to ductile-mode cutting on all crystallographic orientations. Taking into account slip system and cleavage, it could be possible to predict the surface quality.

4. Ultra-precision cylindrical turning

4.1. Experimental procedure

Cylindrical turning was carried out by the ultra-precision aspheric surface machine tool (ULG-100E, TOSHIBA MACHINE) for fabricating optical micro-resonator, as shown in Fig. 7. The CaF_2 workpieces (with a 6 mm diameter and 30 mm length) with end face orientations (1 1 1), (1 1 0), and (1 0 0) were prepared. Fig. 8(a) shows the experimental setup for cylindrical turning. A workpiece fixed with a brass jig was mounted onto the vacuum chucks. Firstly, brittle region rough turning was performed to form the 1 mm diameter under the following cutting conditions: 1000 min^{-1} rotation speed, 20 μm/rev feed per revolution, and 2 μm depth of cut. Afterward, pre-finish cutting was performed to remove the large cracks under the following cutting conditions: 1000 min^{-1} rotation speed, 3 μm/rev feed per revolution, and 100 nm depth of cut. Finally, ductile-mode finish cutting was performed under the condition shown in Table 3. As a result, the total removal thickness in finish cutting was set to 6 μm.

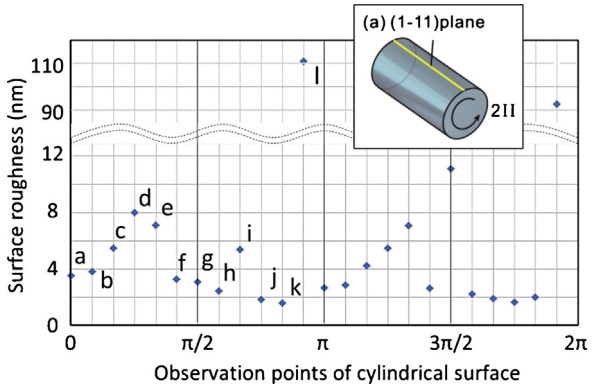

Fig. 14. Cylindrical surface roughness after turning with end face (1 1 0).

According to the abovementioned orthogonal cutting test, the depth of cut could be set at 50 nm to produce a homogeneous ductile surface on all crystallographic orientations. In addition, from the previous research [19], it was found that the feed per revolution in the range of 0.1–0.7 μm/rev does not affect the machined cylindrical surfaces at the 50 nm depth of cut. Hence, 0.3 μm/rev feed per revolution was employed in the finish condition. The scanning electron microscope image of the single-crystal diamond tool (with a 0.2 mm nose radius, −20° rake [18], and 8° clearance) is shown in Fig. 8(b). Fig. 9 shows the observed machined surfaces from the view of each end face, viewed through the optical microscope (VH-Z100UR, KEYENCE) and scanning white light interferometer (New View TM6200, Zygo).

4.2. Experimental results and discussion

4.2.1. End face orientation (1 1 1)

Surface roughness seemed to depend on crystal anisotropy (Fig. 10). Fig. 11 shows the cylindrical machined surfaces measured at 15° intervals at the criterion plane of (a) (01−1). Fig. 12 represents the corresponding crystallographic images of the

Table 3
Finish turning conditions.

Cutting speed m/min:	3.14	Depth of cut nm:	50
Rotation speed min-1:	1000	Removed thickness μm:	1.0
Feed μm/rev:	0.3	End face:	(1 1 1), (1 1 0), (1 0 0)

cylindrical surfaces. At this crystal structure, its cycle was 120° when taking into account the symmetry structure and surface roughness value. According to the orthogonal cutting test of the (1 1 0) plane, the critical depth of cut in a [−1 1 1] and [−1 −1 1] direction was over 500 nm. Because of this, the machined surfaces of (a) and (e) were smooth with no micro-cracks. In the machined surfaces of (b), (c), (f), and (g), cracks appeared along the cleavage plane's side-line. The cutting stress state of brittle cutting region cutting has previously been discussed by Yan [20]. In cylindrical rough turning, there exists a concentration region of tensile stress in front of the diamond tool [21,22]. This tensile stress could be accumulated by repeated rough turning and be liable to cause cleavage and deeper cracks (Fig. 13). The deeper cracks with a thickness larger than 6 μm could not be removed after finish turning. More

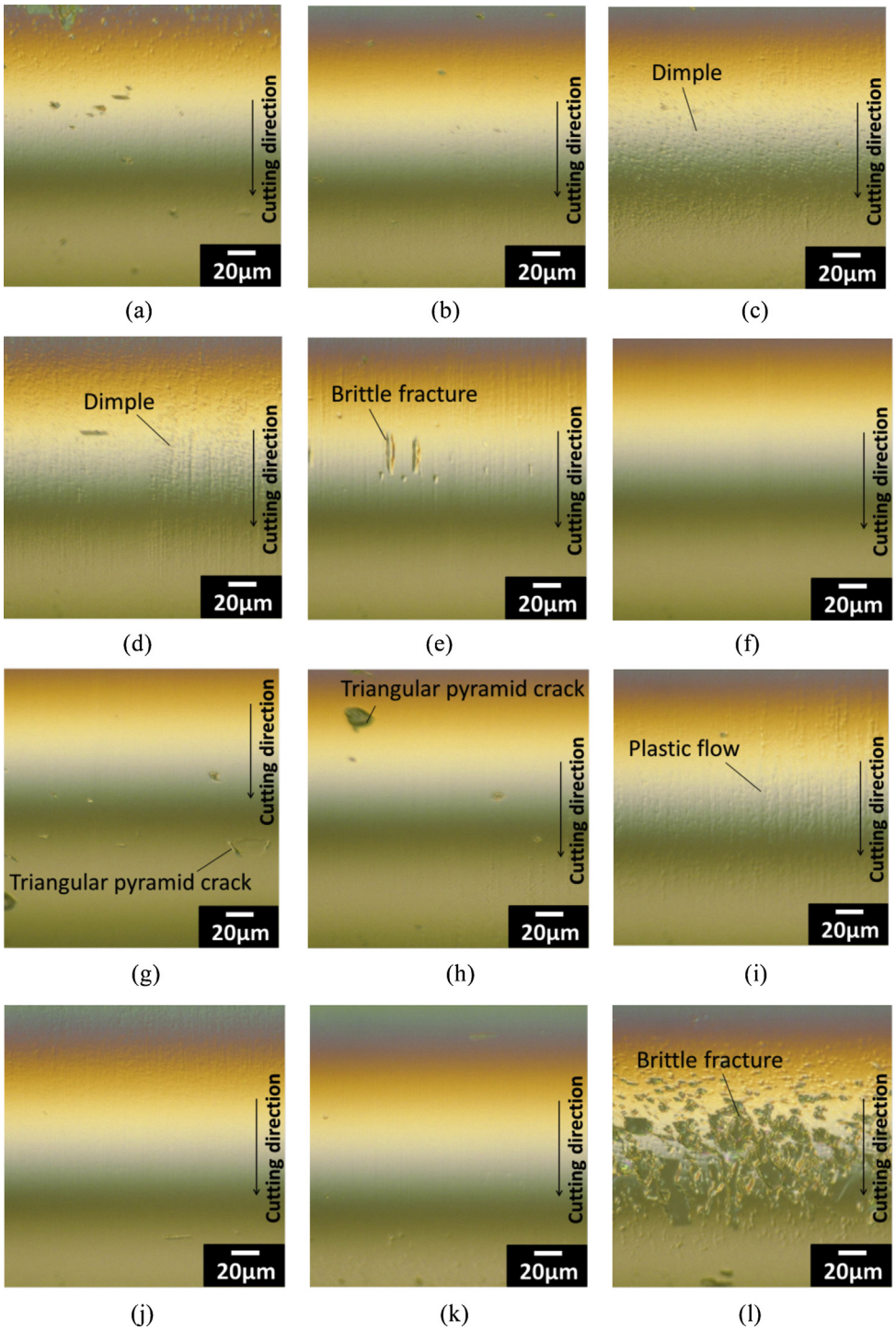

Fig. 15. Machined cylindrical surfaces with end face (1 1 0), for (a) (1 1 1)[1 −1 −2], (b) (23 −23 12)[6 −6 23], (c) (4 −4 −1)[−1 1 −8], (d) (4 −4 −1)[−1 1 −8], (e) (3 −3 −2)[−1 1 −3], (f) (40 −40 −47)[−1 0 1 0 −17], (g) (1 −1 −2)[−1 1 −1], (h) (6 −6 −23)[−1 9 1 9 −10], (i) (3 −3 46)[−2 3 2 3 −3], (j) (−44 −33)[−44 1], (k) (−1 1 −3)[−3 3 2], and (l) (−1 0 1 0 −17)[−6 6 7].

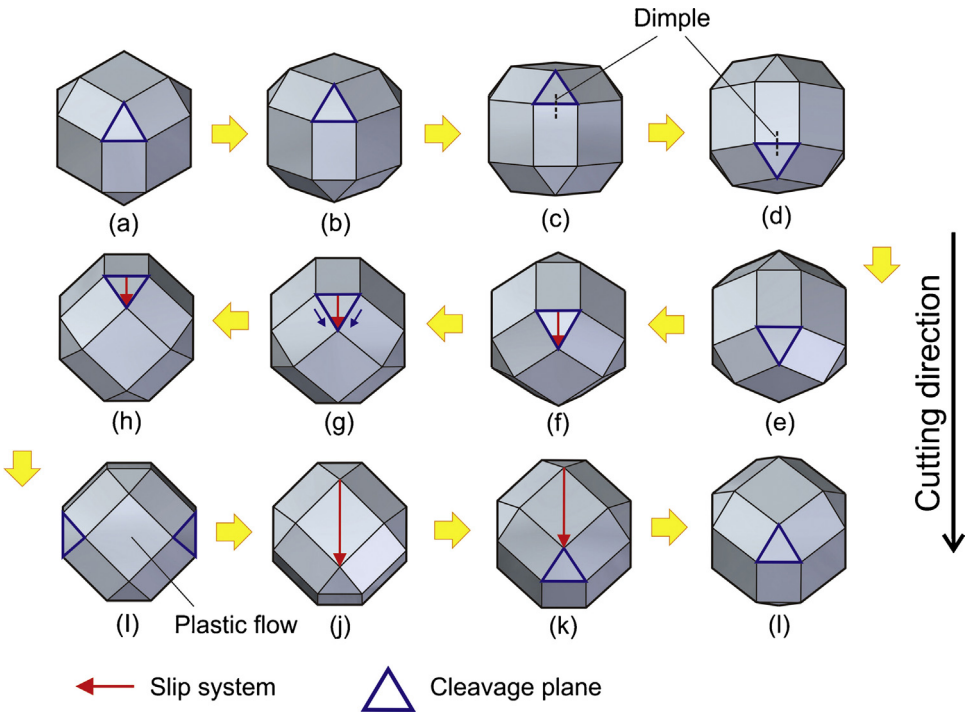

Fig. 16. Crystallographic images of machined cylindrical surfaces with end face (1 1 0), for (a) (1 1 1)[1 −1 −2], (b) (23 −2 3 1 2)[6 −6 2 3], (c) (4 −4 −1)[−1 1 −8], (d) (4 −4 −1)[−1 1 −8], (e) (3 −3 −2)[−1 1 −3], (f) (40 −40 −47)[−1 0 1 0 −1 7], (g) (1 −1 −2)[−1 1 −1], (h) (6 −6 −23)[−1 9 1 9 −10], (i) (3 −3 46)[−2 3 2 3 −3], (j) (−44 −33)[−44 1], (k) (−1 1 −3)[−3 3 2], and (l) (−10 10 −17)[−6 6 7].

finish cutting processes were needed to remove all cracks, which resulted in lower resonator production efficiency.

4.2.2. End face orientation (1 1 0)

From Fig. 14, it is clear that surface roughness strongly depended on crystal anisotropy. Figs. 15 and 16 show the cylindrical machined surfaces at 15° intervals for the criterion plane (a) (1 −1 1) and the corresponding crystallographic images. From the relation between the symmetry structure and surface roughness, it appeared that this crystal structure's cycle was 180°. In the surfaces (a) and (f), the cutting plane was the same as the cleavage plane, nevertheless the surface quality was different. The same tendency existed for the orthogonal cutting test of a (1 1 1) plane. The critical depth of cut on the (f) surface was around 600 nm, while that on the (a) surface was below 100 nm. A crack shaped like a triangular pyramid was observed in the images of the (g) and (h) surfaces. The shape might conceivably emanate along a (1 −1 −1) cleavage plane. In the surfaces of (c) and (d), cracks like dimples were observed. According to the micro-Vickers hardness test, cracks tended to be easily initiated on a (1 1 0) plane. Similarly, in cylindrical turning the negative rake face made the material extruded like the indenter probe and the thrust force could be vertically applied to a (1 1 0) plane. In the surfaces of (j) and (k), the slip system of (0 0 −1)[−1 1 0] contributed to the smooth surfaces, which was consistent with the result of the orthogonal cutting test on the (1 0 0) plane. On the other hand, in the surface of (i), the surface quality was not good, although the slip system of (0 0 −1)[−1 1 0] should theoretically take place. Plastic flow appeared to be obtained instead of cracks. It was conceivable that the crystal property could be changed at the switching point of the slip system. Additional studies are however required. In the surfaces of (e) and (l), it was clear that large cracks remained even after ductile region finish turning. When the cutting force was applied along the cleavage plane, the thrust force is likely to cleave the surface vertically. Actually, approximately 15 μm depth of cracks remained, which was larger than the total removed thickness of finish turning. In spite of the ductile mode cutting condition at 50 nm depth of cut, a whole fine surface could not be achieved. This would be because of the difference in cutting speed. High cutting speed might increase the influence of crystal anisotropy on the machined surface quality, because it was found that the critical depth of cut tended to decrease with increasing cutting speed in CaF_2 cutting [23]. Crystal structure with end face orientation (1 1 0) was therefore not suitable for resonator production.

4.2.3. End face orientation (1 0 0)

Surface roughness is shown in Fig. 17. Figs. 18 and 19 show the cylindrical machined surfaces at 15° intervals at the criterion plane of (a) (0 1 0) and the corresponding crystallographic

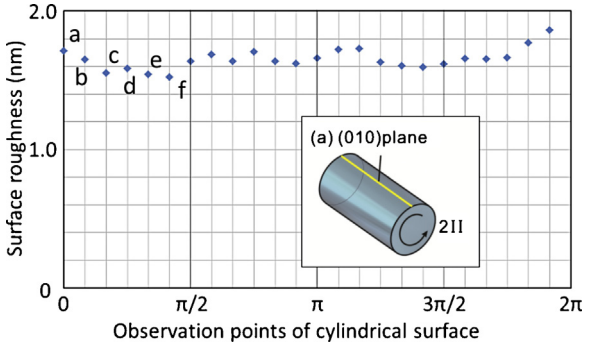

Fig. 17. Cylindrical surface roughness after turning with end face (1 0 0).

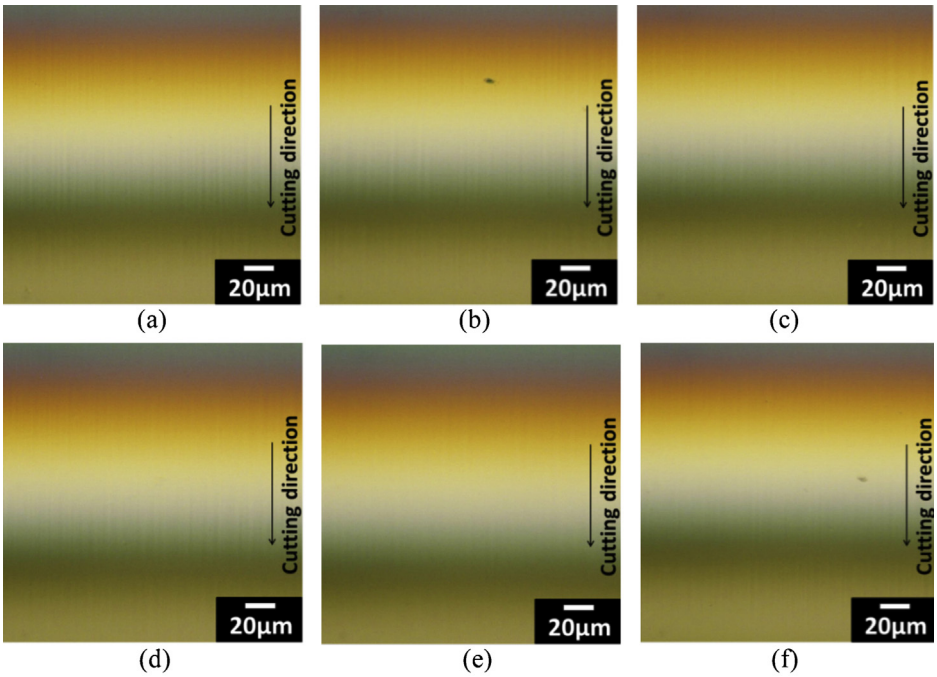

Fig. 18. Machined cylindrical surfaces with end face (100), for (a) (010)[001], (b) (0154)[0−415], (c) (074)[0−47], (d) (011)[0−1−1], (e) (047)[0−74], and (f) (0415)[0−154].

images. At this crystal structure, its cycle was 90°, when taking the symmetry structure and surface roughness into account. Unlike for the other workpieces, such as end face orientation (111) and (110), smooth surfaces could be achieved without cracks and the surface roughness was below 1.7 nm. From a mechanics and crystallography perspective, cutting force could be evenly distributed on the cleavage planes arranged on both sides, because of the mirror symmetry structure of end face orientation (100) (Fig. 20). This crystal structure enabled a smooth surface throughout the whole cylindrical surface. The crystal structure was therefore the most suitable for CaF_2 optical resonator fabrication.

Based on this study, a future outlook can finally be introduced. Some crystal planes seemed to be simultaneously affected by the slip system and cleavage. To analyze the cutting mechanism in detail, atomic density or filling rate at atomic level should be taken into account. Furthermore, at the resonator manufacturing stage, it is effective to evaluate the relationship between subsurface damage and resonator performance.

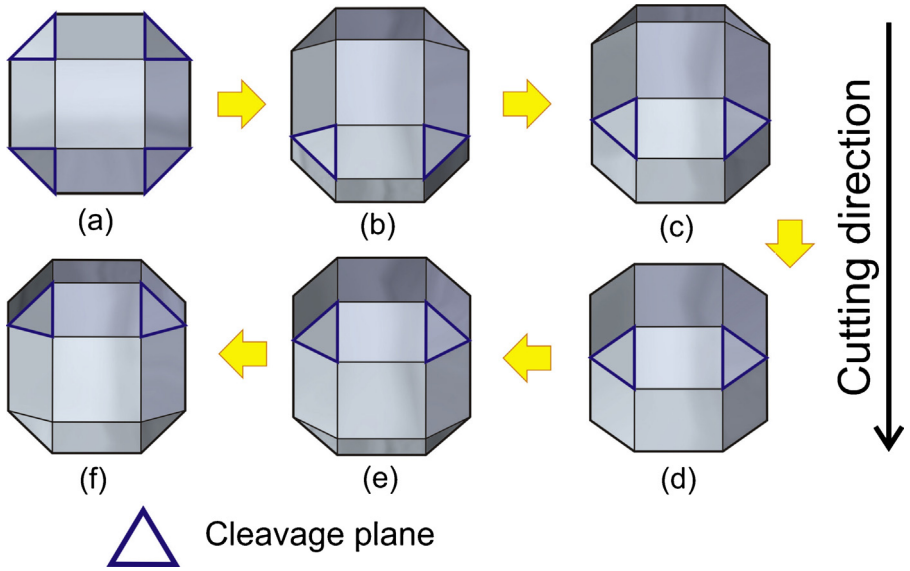

Fig. 19. Crystallographic images of machined cylindrical surfaces with end face (100), for (a) (010)[001], (b) (0154)[0−415], (c) (074)[0−47], (d) (011)[0−1−1], (e) (047)[0−74], and (f) (0415)[0−154].

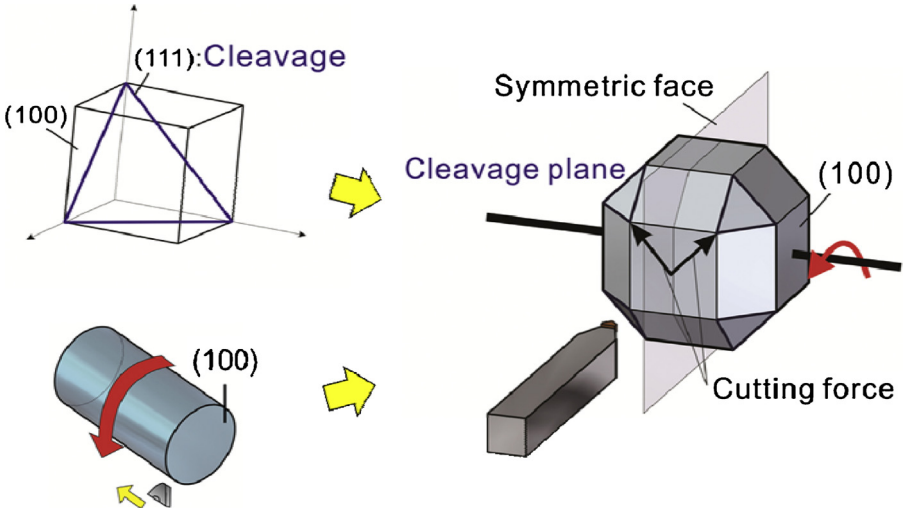

Fig. 20. Distribution of cutting force in the mirror symmetry structure.

5. Conclusions

This study focused on ultra-precision machining of single-crystal CaF_2 to be able to manufacture optical micro-resonators more efficiently. We analyzed surface quality and crack initiation, in terms of slip system and cleavage, through three experiments: a micro-Vickers test, an orthogonal cutting test, and ultra-precision cylindrical turning. The following conclusions were drawn:

1. The micro-Vickers test revealed that plastic deformability varied according to crystal orientation. Plastic deformation was generated more easily and cracks tended not to appear on the (1 0 0) plane compared to the (1 1 1) and (1 1 0) planes.
2. The orthogonal cutting tests revealed that critical depth of cut tended to become deeper when the cutting direction corresponded to the slip system. It could be possible to predict surface quality after cutting when taking the crystal structure into account.
3. In cylindrical turning, deeper cracks with a thickness above 6 μm remained even after finish turning. This could be because tensile stress was accumulated by repeated brittle mode rough turning.
4. A smooth surface could be achieved throughout the whole cylindrical surfaces of CaF_2's crystal structure with end face orientation (1 0 0). The cutting force could be evenly distributed on the cleavage planes because of its mirror symmetry structure.

In future, the atomic density or filling rate on machined surfaces needs to be considered. It is effective to evaluate the relation between subsurface damage and resonator performance at the resonator manufacturing stage.

Acknowledgements

The authors gratefully acknowledge technical support from Dr. Katsutoshi Tanaka and Dr. Masahiko Fukuda of TOSHIBA MACHINE CO., LTD. This study was partially supported by the Takahashi Industrial and Economic Research Foundation. The authors would like to express their sincere appreciation for the support.

References

[1] Armani DK, Kippenberg TJ, Spillane SM, Vahala KJ. Ultra-high-Q toroid microcavity on a chip. Nature 2003;421:925–8.
[2] Tanabe T, Notomi M, Kuramochi E, Shinya A, Taniyama H. Trapping and delaying photons for one nanosecond in an ultra-small high-Q photonic-crystal nanocavity. Nat Photon 2007;1:49–52.
[3] Vollmer F, Arnold S. Whispering-gallery-mode biosensing: label-free detection down to single molecules. Nat Methods 2008;5(7):591–6.
[4] Savchenkov AA, Ilchenko VS, Matsko AB, Maleki L. Kilohertz optical resonances in dielectric crystal cavities. Phys Rev A 2004;70:051804(R).
[5] Kudo H, Ogawa Y, Kato T, Yokoo A, Tanabe T. Fabrication of whispering gallery mode cavity using crystal growth. Appl Phys Lett 2013;102:211105.
[6] Grudinin IS, Matsko AB, Savchenkov AA, Strekalov D, Ilchenko VS, Maleki L. Ultra high Q crystalline microcavities. Opt Commun 2006;265:33–8.
[7] Maleki L, Ilchenko VS, Savchenkov AA, Matsko AB. Crystalline whispering gallery mode resonators in optics and photonics. In: Matsko AB, editor. Practical applications of microresonators in optics and photonics, 3. Boca Raton, FL, USA: CRC Press, Taylor & Francis Group; 2009. p. 133–210.
[8] Matsumura T, Aristimunob P, Gandariasb E, Arrazolab PJ. Cutting process in glass peripheral milling. J Mater Process Technol 2013;213:1523–31.
[9] Foy K, Wei Z, Matsumura T, Huang Y. Effect of tilt angle on cutting regime transition in glass micromilling. Int J Mach Tools Manuf 2009;49:315–24.
[10] Tang X, Nakamoto K, Obata K, Takeuchi Y. Ultraprecision micromachining of hard material with tool wear suppression by using diamond tool with special chamfer. CIRP Ann Manuf Technol 2013;62:51–4.
[11] Takeuchi Y, Sawada K, Saito T. Ultraprecision 3D micromachining of glass. CIRP Ann Manuf Technol 1996;45(1):401–4.
[12] Namba Y, Ohnishi N, Yoshida S, Harada K, Yoshida K. Ultra-precision float polishing of calcium fluoride single crystals for deep ultra violet applications. Ann CIRP 2004;53(1):459–62.
[13] Namba Y, Yoshida T, Yoshida S, Yoshida K. Surfaces of calcium fluoride single crystals ground with an ultra-precision surface grinder. CIRP Ann Manuf Technol 2005;54(1):503–6.
[14] Min S, Lee D-E, de Grave A, De Oliveira Valente CM, Lin J, Dornfeld DA. Surface and edge quality variation in precision machining of single crystal and polycrystalline materials. Proc Inst Mech Eng B J Eng Manuf 2006;220:479.
[15] Yan J, Syoji K, Tamaki J. Crystallographic effects in micro/nanomchining of single-crystal calcium fluoride. JVST B Microelectron Nanometer Struct 2004;22(1):46–51.
[16] Lodes MS, Hartmaier A, Goken M, Durst K. Influence of dislocation density on the pop-in behavior and indentation size effect in CaF_2 single crystals: experiments and molecular dynamics simulations. Acta Mater 2011;59:4246–73.
[17] Takechi T, Tamaki J. Elastic behavior and plastic behavior in ductile-regime fixed-abrasive machining of optical glass. J Jpn Soc Abras Technol 2011;55(2):113–20.
[18] Yan J, Tamaki J, Syoji K, Kuriyagawa T. Single-point diamond turning of CaF_2 for nanometric surface. Int J Adv Manuf Technol 2004;24:640–6.
[19] Azami S, Kudo H, Tanabe T, Yan J, Kakinuma Y. Basic study of ultra-precision turning of single-crystal calcium fluoride based on crystal anisotropy. Jpn Soc Precis Eng 2013;60:601–2.
[20] Yan J, Syoji K, Kuriyagawa T, Suzuki H. Ductile region turning at large tool feed. J Mater Process Technol 2002;121:363–72.
[21] Fang FZ, Wu H, Liu YC. Modelling and experimental investigation on nanometric cutting of monocrystalline silicon. Int J Mach Tools Manuf 2005;45:1681–6.
[22] Wiston SB, Ronald OS. Crystal orientation dependence of machining damage: a stress model. J Am Ceram Soc 2005;73(10):3113–5.
[23] Mizumoto Y, Aoyama T, Kakinuma Y. Basic study on ultraprecision machining of single-crystal calcium fluoride. Proc Eng 2011;19:264–9.